doi.org/10.52568/001805/JCSP/47.06.2025

Synthesis of Bioactive Benzofuran Derivatives *via* Suzuki –Miyaura Cross-Coupling Reaction

Lal Khan and Muhammad Zubair*
Department of Chemistry, Government College University Faisalabad, 38000, Pakistan.
Zubairmkn@gcuf.edu.pk*

(Received on 17th Feb 2025, accepted in revised form 30th September 2025)

Summary: Suzuki–Miyuara coupling facilitated the synthesis of phenylbenzofuran-2-carboxylate analogs (**5a–5h**). The structural characteristics of the target molecules were examined through a range of computational methodologies, such as molecular docking and DFT studies. Through computational studies, target molecules underwent additional screening for hemolytic, antibacterial (both gram-positive and gram-negative), and enzyme inhibitory activities, such as anti-urease and *α*-glucosidase, to assess their biological potential. The hemolytic results for compounds **(5a–5h)** indicated their nontoxicity towards RBCs. Notably, compound **(5g)** showed the highest antibacterial activity **9**mm and compound **(5b)** displayed substantial efficacy against E. coli, demonstrating a zone of inhibition measuring **5**mm in comparison to the standard drug ciprofloxacin. Moreover, Compound **(5d)** demonstrated a moderate level of antibacterial activity, measuring **4** mm against Gram-positive bacteria (B. subtilis). Notably, compounds (**5b)** and (**5a**) demonstrated remarkable inhibitory potential against urease and α-glucosidase (IC_{50} = 66.83 ± 1.66µM, IC_{50} = 47.3 ± 2.30µM), respectively, which are comparable to those of standard drugs. The predictions derived from DFT and molecular docking regarding structural features corroborated the experimental findings. The findings indicate that computational and *in vitro* studies serve as the most effective methodologies for the molecular screening of drug candidates.

Graphical Abstract

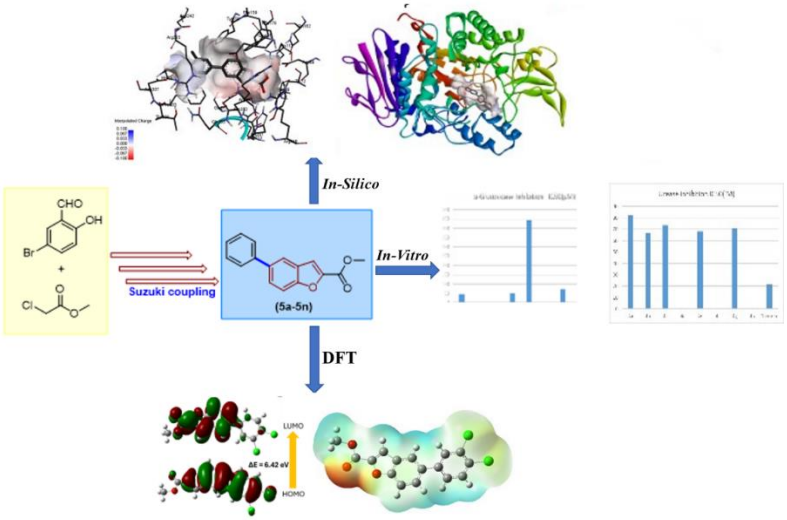

Keywords: Suzuki–Miyaura reaction, benzofuran, Molecular Docking, Anti-urease, *α*-glucosidase, DFT studies

Introduction

Diabetes mellitus, a protruding metabolic syndrome affecting 422 million individuals globally and causes severe linked problems like heart, and kidney diseases, nervous disorders, retinopathy, and leg amputation [1, 2]. *Helicobacter pylori* is recognized as a significant gastroduodenal pathogen because of its causal relationship with gastric and duodenal diseases. A strong correlation was observed between blood urea levels and both the duration and severity of diabetes [3, 4]. *α*-Glucosidase is a viable target potential to tackle this outcome and seek medicinal chemists' attention significantly across the globe [5, 6]. The α-glucosidase enzyme is located in the epithelium of small intestine, where it facilitates

*To whom all correspondence should be addressed.

the breakdown of disaccharides and starch into glucose, enabling absorption into the bloodstream. The hydrolytic cleavage rate of oligosaccharides into monosaccharides is impeded when the intestinal α-glucosidase enzyme is inhibited [7, 8]. Multimorbidity such as diabetes mellitus and H. pylori infections have prompted an exploration for drugs that can target multiple pathways [9-11]. In this context, heterocycles, whether derived from natural sources or synthesized, emerge as a primary option due to their extensive range of applications. Benzofuran compounds, a type of heterocycle, are naturally abundant and serve as fundamental structural units for a diverse array of naturally occurring molecules, showcasing multidirectional functionalities. A variety of studies have documented the properties of benzofurans derivatives, highlighting their potential as anti-tumor, anti-oxidative, anti-bacterial, and anti-viral agents [12, 13]. The synthesis of substituted benzofurans, iso-benzofuran, and spiro-benzofuran involves a variety of reaction [14]. These compounds are important intermediates for the synthesis of a variety of useful and novel heterocyclic systems that are otherwise difficult to obtain synthetically [14, 40, 41].

Furochromone like khellin and visnagin act as secondary metabolites, isolated from medicinal plant '*Ammi visnage Lam'* are synthesized from benzofuran derivatives. Benzofuran derivatives showed potent vasodilatatory, hypotensive, antibacterial, antifungal, antiparasitic activities [42]. Furochromone derivatives acts as synthetic targets having important biological activities as anti-atherosclerotic and lipid altering activity [43]. Khellin has been used in the photo-chemotherapeutic treatment of vitiligo and psoriasis (43). Furochromone derivatives are reported as anti-atherosclerotic, antineoplastic, anti-gastric, anti-anaphylactic and are used in the treatment of urolithiasis, hypertriglyceridemia and vitiligo [44]. Furochromone and benzofurans derivatives are used as antiviral and anticancer activities. Furochromone fused with pyrimidine, quinoxaline and pyrazole derivatives showed anti-inflammatory and analgesic activities, the cytotoxic activity and used in the protection of DNA [44]. Triazolopyrimidine and Furochromone have a wide range of pharmacological activities for the treatment of numerous diseases, including anticancer, antiviral, anti-depressant, anti-microbial, anti-inflammatory, and analgesic activities [45].

Among these, the Suzuki-Miyaura reaction is commonly utilized for the desired cross-coupling reaction in organic and medicinal chemistry. Suzuki cross coupling reactions are used in organic synthesis to create biologically active compounds such as benzofuran [15, 16].

This work examines the synthesis of functionalized benzofuran esters by the Suzuki-Miyaura cross-coupling process, a promising technique for synthesizing C-C bonds with excellent efficiency and selectivity. The addition of various substituents to benzofuran functionality increases the compounds' pharmacological potential, making them intriguing candidates for antibacterial, α-Glucosidase, and anti-urease inhibitors. Further, Density Functional Theory (DFT) carried out to determine the detailed structural analysis, molecular geometry, electronic characteristics, and stability of the synthesized benzofuran esters (**5a-5h**). However, the integration of synthetic method and computational validation emphasizes the importance of benzofuran esters in drug development scaffolds for building therapeutic potentials.

Experimental

Antibacterial potential of compounds

Antibacterial efficacy of all produced compounds was assessed by *in vitro* tests against *Escherichia coli*/*Bacillus subtilis*, exhibiting gram-negative and positive bacteria. The first antibacterial efficacy were assessed using agar well diffusion protocol [17]. Ciprofloxacin serves as a referenc e medication for comparative analysis. The evaluated chemicals were solubilized in dimethyl sulfoxide (DMSO) to achieve concentrations of 50% and 100%. The samples were immediately inserted into the wells of the agar plate. The plates containing bacteria were cultured at 37°C for 24 hours. Every experiment was conducted in triplicate. Average inhibition zone diameter around well, taken in millimeters, was recorded for each tested substance [18].

Computational Methods

The energy associated with the optimized geometry of the synthesized molecules (**5a–5h**) was computed utilizing Gaussian software, employing DFT parameters of the B3LYP/6-31G model [19]. The three-parameter exchange function developed by Becke, commonly referred to as B3LYP, is extensively employed in quantum chemical calculations owing to its reliable performance when paired with the nonlocal correlation function proposed by Lee, Yang, and Parr [20, 21]. The preliminary molecular geometry of the examined molecule was determined through experimental single crystal X-ray analysis. The identical calculations employing the B3LYP method

alongside the 6-31G basis set were utilized to derive the optimized structural parameters [22]. All calculations were conducted using Gaussian 16 [23]. Gauss View 6 served as the graphical interface for visualizing the optimized geometry, HOMO-LUMO, and Molecular Electrostatic Potential (MEP) [24, 25].

Structural Interaction Analysis (Molecular Docking)

For docking studies, the ligand and receptor protein structures were meticulously processed utilizing Avogadro version 1.2.0 and BioVIA Discovery Studio Visualizer v21.1 (DSV) [26]. The geometry of each synthesized ligand underwent optimization utilizing Merck Molecular Force Field parameters. In the process of docking, the grid surface was meticulously calibrated to encompass the entirety of the receptor, centering it appropriately. This was accomplished utilizing the Auto Dock Tools version 1.5.7 (ADT) software package [27]. Standard docking parameters were established for the docking of all ligands with the receptor. A genetic search algorithm was employed to determine the interacting energy and affinity across the ligand and receptor. The conformation exhibiting the minimal energy was chosen as the most stable for subsequent post-docking analysis. The inhibition constant (Ki) was subsequently determined utilizing Equation 1.

$$\Delta G = RT \ln Ki \quad (1)$$

$$Ki = e(\Delta G/RT)$$

where ΔG represents the binding affinity or energy in Kcal/mol, Hence, R denotes the gas constant, 1.987 cal/mol/K, and T corresponds to room temperature, 298.15 K. The analysis of ADT results was conducted utilizing Python Molecular Viewer 1.5.7 and DSV. Interactions between ligands and receptors involving various atoms and functional groups were also noted. A docking score characterized by low kinase inhibition (KI μM) and a more stable conformation of the ligand with the receptor was employed for the docking analysis.

Enzymatic Activity of Compounds

Inhibition of Urease

The assessment of urease inhibitory activity for compounds (**5a–5h**) was conducted using established methodologies. The procedure involves a reaction mixture consisting of 25 μL solution of jack bean urease enzymes and containing 100 mM urea of phosphate buffer 55μL, which was incubated with 5 μL of the test derivatives (**5a-5h**) (0.5 mM) for 15 minutes in 96-well plates at 30 °C [28, 29]. The assessment of ammonia production was carried out utilizing Weather burn's (1967) indophenol method, facilitating the evaluation of urease activity [30]. In summary, each well was supplemented with 70 μL of an alkaline substrate, which included 0.5% w/v NaOH/0.1% active chloride NaOCl, in conjunction with 45 μL of the phenolic substrate, composed of 1% w/v phenol and 0.05% w/v sodium nitroprusside, resulting in 200 μL total volume. The absorbance recorded at 630 nm demonstrated an elevation following a period of 50 minutes, employing a microplate reader (Spectra Max, Molecular Devices, USA). Conducted a thorough analysis of the results, specifically the change in absorbance per minute, employing SoftMax Pro software from Molecular Devices, USA. The comprehensive assessment was conducted in triplicate at a pH of 6.8. The standard control employed was thiourea [31].

The calculation of the percentage of inhibition is derived from the subsequent equation:

$$100 - (ODtestwell/ODcontrol) \times 100 \quad (2)$$

α-Glucosidase Inhibition

The target molecules (**5a–5h**) underwent in-vitro α-glucosidase inhibition studies conducted in 96 microwell plates, employing the methodology previously delineated. Each well was filled with 100 μL of a 100 mM pH-6 phosphate buffer, followed by the addition of 50 μL of a commercial solution of Saccharomyces cerevisiae α-glucosidase at a concentration of 1 U/mL, with a slight modification to the procedure. Each compound was individually dissolved in DMSO (10 μL) and subsequently added to the designated well, followed by incubation of the microplate at 37 °C for a duration of 10 minutes. Subsequently, 40 μL p-nitrophenyl-α-D-glucopyranoside (p-NPG) in 5 mM solution was introduced into each well, and the mixture was incubated once more at 37 °C for a duration of 10 minutes. A volume of 100 μL from a 0.5 M Tris solution was employed to halt the reaction, utilizing a Molecular Devices USA Spectra Max spectrometer, which was calibrated for the detection of p-nitrophenol release at a wavelength of 405 nm. The efficacy of the synthesized analogs was evaluated in relation to acarbose, which served as a reference point [32]. Each experiment was conducted thrice, utilizing inhibitor-free reaction mixtures as negative controls. The calculation of percent inhibition or activity is derived from Equation 2.

For the preliminary assessment, a concentration of 200 μM was employed to inhibit *α*-

glucosidase. The IC_{50} value was subsequently ascertained through the application of suitable concentrations alongside the screened compounds exhibiting a significant percentage of inhibition.

Hemolytic potential of compounds

The hemolytic potential of synthesized analogs (**5a-5h**) was checked using the known methods [33, 34]. Three milliliters of newly acquired, heparinized cow blood collected from Clinical Medicine and Surgery Department at Agriculture Faisalabad in Faisalabad, Pakistan. For five minutes, after centrifuging the blood at 1000xg, the plasma was removed, and the cellular components were subjected to a tri-fold washing procedure with five milliliters of sterile, isotonic PBS (pH 7.4) chilled to four degrees Celsius. Maintained the preservation of 108 cells per milliliter of erythrocytes for each testing performed. Each substance was amalgamated with 100 µL of human cells per mL in a regulated setting. Samples were incubated at 37 °C for 35 minutes, then undergoing centrifugation for 10 minutes. Thereafter, they were cooled on ice for five minutes and were centrifuged for an additional five minutes at a speed of 1000xg. One hundred microliters of the supernatant were taken from each tube and then diluted tenfold with cold phosphate-buffered saline at 4 degrees Celsius. Phosphate-buffered saline (PBS) functions taken as negative control, whilst 0.1% v/v Triton X-100 taken as positive control; both underwent similar procedural protocols. Absorbance was evaluated at 576 nm using µQuant (Bioteck, USA). The percentage of RBC lysis was determined for each sample.

Synthetic protocol for Methyl 5-bromo-1H-indene-2-carboxylate **(3).**

An ester derived from benzofuran was synthesized through the reaction of bromo salicylaldehyde (2g, 0.016 moles) with methyl chloroacetate (1.191g, 0.0176 moles), utilizing DMF as the solvent and K_2CO_3 (2.43g, 0.0176 moles) as the base. The reaction mixture underwent reflux for a duration of six to eight hours using a sand bath. Upon the completion of the reaction, the final product was meticulously isolated through the addition of ice-cold distilled water. Refine utilizing column chromatography (Scheme 1).

Mechanism of the Suzuki Cross-Coupling reaction.

The Suzuki coupling reaction process comprises a palladium-catalyzed cross-coupling of an organoboron compound with an aryl or vinyl halide to produce a new carbon-carbon bond. The reaction progresses via a catalytic cycle that includes three major steps: oxidative addition, transmetallation, and reductive elimination

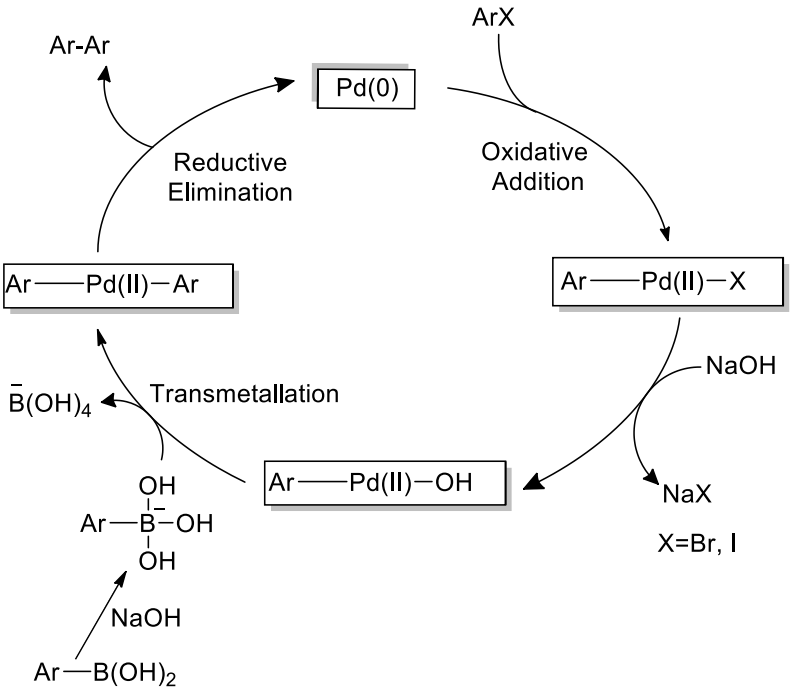

Fig. 2: Catalytic cycle for Suzuki cross coupling reaction.

Comprehensive methodology for the synthesis of compounds **(5a-5h)**

In a Schelling flask, 0.15 g (0.46 mmol) of ester and 0.035 g (5 mol %) of palladium were added. Following this, 5–6 milliliters of 1,4-dioxane solvent were added, and the mixture was then agitated under an inert environment for 30–45 minutes. Then, distilled water, aryl boronic acid (1.1 equivalents), and potassium bicarbonate (2.2 equivalents) were added as the base. An extra 12–16 hours were added to the reflux time of the reaction mixture (Fig 2). Through the use of thin-layer chromatography, the reaction's course could be monitored. A 9:1 solvent combination of n-hexane and ethyl acetate was used in column chromatography to separate the product when the reaction was finished. After the solvent was evaporated using a rotary evaporator, the solid product was produced [35].

Spectral Analysis

*Methyl 5-(4-(methoxycarbonyl) phenyl)benzofuran-2-carboxylate***(5a).**Start with compound **3** (0.15 g, 0.598 mmol), Catalyst Pd(PPh_3) (0.035 g, 2.99 mmol), base K_3PO_4 (0.13 g, 0.126 mmol), and 4-methoxy phenyl boronic acid, (0.12 g, 0.68mmol).Yield 60%, Colorless solid, mp :137-138 °C ^{1}H NMR (400 MHz, $CDCl_3$, δ ppm, *J* Hz): 3.93 (3H, s,OCH_3), 3.98 (3H, s, OCH_3) , 7.52 (1H, m, ArH), 7.56 (1H, s, ArH), 7.65 (2H, d, *J*=8, ArH), 7.68 (1H, d, *J*=8, ArH), 7.88 (1H, s, ArH), 8.10 (2 H,d, *J*=8, ArH); ^{13}C NMR (101 MHz, $CDCl_3$): 52.16 (OCH_3), 52.49 (OCH_3), 112.73 (CH), 113.85 (CH), 114.5 (CH), 121.44 (CH), 127.29 (CH), 127.40 (CH), 127.54 (CH), 128.89 (CH), 130.17 (C), 130.67 (C), 136.34 (C), 145.26 (C), 146.20 (C), 155.58 (C), 159.79 (C), 116.92 (C)

*Methyl 5-(4-chlorophenyl)benzofuran-2-carboxylate***(5b).**Starting with molecule **3** (0.15 g, 0.598 mmol), catalyst Pd(PPh_3) (0.035 g, 2.99 mmol), base K_3PO_4 (0.13 g, 0.126 mmol), and 4-$ClC_6H_5B(OH)_2$, (0.106 g, 0.68mmol).Yield 67, Colorless solid, mp :126 - 127°C ^{1}H NMR (400 MHz, $CDCl_3$, δ ppm, *J* Hz): 3.96 (3H, s, OCH_3), 7.55 (1H, s, ArH), 7.63 (1H, d, *J*=8, ArH), 7.80 (1H, s, ArH), 7.40 (2H, d, *J*=8, ArH), 7.45(1H, d, *J*=8 ArH), 7.50 (2H, d, *J*=8, ArH); ^{13}C NMR (101 MHz, $CDCl_3$): 21.40 (CH_3), 52.41 (OCH_3), 112.33 (CH), 114.19 (CH), 121.01 (C), 125.35 (CH), 127.33 (CH), 127.59 (CH), 128.89 (CH), 137.81 (C), 138.38 (C), 140.85 (C), 145.85 (C), 155.70 (C),159.93 (C).

Methyl 5-(3-chlorophenyl)benzofuran-2-carboxylate **(5c).**Starting with molecule **3** (0.15 g, 0.598 mmol), Catalyst Pd(PPh_3) (0.035 g, 2.99 mmol), K_3PO_4 (0.13 g, 0.126 mmol), and 3-$ClC_6H_4B(OH)_2$, (0.106 g, 0.68mmol).Yield 66%, Colorless solid, mp : 115°C ^{1}H NMR (400 MHz, $CDCl_3$, δ ppm, *J* Hz): 3.98 (3H, s, OCH_3), 7.51 (1H, s, ArH), 7.37 (1H, d, *J*=8, ArH), 7.45 (1H, d, *J*=8, ArH), 7.33 (1H, t, ArH), 7.60 (1H, s, ArH), 7.56 (1H, d, *J*=8, ArH), 7.64 (1H, d, *J*=8, ArH), 7.82 (1H, s, ArH); ^{13}C NMR (101 MHz, $CDCl_3$): 52.48 (OCH_3), 112.68 (CH), 114.05 (CH), 121.22 (C), 125.55 (CH), 127.29 (CH), 127.50 (CH), 127.53 (CH), 130.07 (CH), 130.67 (CH), 134.71 (C), 136.15 (C), 142.68 (C), 146.15 (C), 155.43 (C), 159.81 (C)

Methyl 5-(3-chloro-4-fluorophenyl)benzofuran-2-carboxylate **(5d).**Starting with molecule **3** (0.15 g, 0.598 mmol), Catalyst Pd(PPh_3) (0.035 g, 2.99 mmol), K_3PO_4 (0.13 g, 0.126mmol), and 3-Cl, 4-F phenyl boronic acid, (0.112 g, 0.68mmol).Yield 62%, Colorless solid, mp : 169°C ^{1}H NMR (400 MHz, $CDCl_3$, δ ppm, *J* Hz): 3.98 (3H, s, OCH_3), 7.78 (1H, s, ArH), 7.19 (1H, d, *J*=8, ArH), 7.42 (1H, m, ArH), 7.55 (1H, s, ArH), 7.59 (1H, m, ArH), 7.62 (1H,d, *J*=4, ArH), 7.64 (1H, s, ArH) ; ^{13}C NMR (101 MHz, $CDCl_3$): 52.53 (OCH_3), 112.74 (CH), 113.95 (CH), 116.79 (CH), 117.00 (C), 121.11 (C), 126.98 (CH), 127.05 (CH), 127.15 (CH), 127.53 (CH), 129.49 (C), 135.37 (C), 138.15 (C), 146.25 (C), 155.34(C), 159.77(C)

Methyl 5-(3-acetylphenyl)benzofuran-2-carboxylate **(5e).**Starting with molecule **3** (0.15 g, 0.598 mmol), Pd(PPh_3) Catalyst (0.035 g, 2.99 mmol), K_3PO_4 (0.13 g, 0.126 mmol), and 4-$MeCOC_6H_4B(OH)_2$, (0.110 g, 0.68mmol).Yield 64%, Colorless solid, mp :164°C ^{1}H NMR (400 MHz, $CDCl_3$, δ p pm, *J* Hz): 3.97 (3H, s, OCH_3), 8.17 (1H, s, ArH), 7.87 (1H, s, ArH), 7.79 (1H, d,J=8, ArH), 7.64 (1H, d, J=8, ArH), 7.93 (1H, t, ArH), 7.53 (1H, d, J=8, ArH), 7.68 (1H, d, J=8, ArH), 7.51 (1H, s, ArH), 2.64 (3H, s, CH_3); ^{13}C NMR (101 MHz, $CDCl_3$): 26.75 (CH_3), 52.45(OCH_3), 112.69 (CH), 114.03(CH), 121.30 (C), 127.10 (CH), 127.40 (CH), 127.36 (CH), 127.54 (CH), 129.13 (C), 131.94 (C), 136.51 (C), 137.67 (C), 141.37 (C), 146.18 (C), 158.80 (C), 197.98 (C)

Methyl 5-(thiophen-2-yl)benzofuran-2-carboxylate **(5f)** Starting with **3** (0.15 g, 0.598 mmol), Pd(PPh_3) Catalyst (0.035 g, 2.99 mmol), K_3PO_4 (0.13 g, 0.126 mmol), and $C_6H_5B(OH)_2$, (0.0829 g, 0.68mmol). Yield 68% Colorless solid, mp321 °C**.** ^{1}H NMR (400 MHz, $CDCl_3$) δ 8.09(1H,s ArH), 7.46(1H, d, *J*=8. ArH),7.54 (1H, t, ArH) 7.48 (1H, d, ArH),7.49 (1H, s, CH), 7.69 (1H, d, *J* = 16.6, 8.6 , ArH), 7.66 (1H, d, *J* = 16.6, 8.6 , ArH),3.55 (3H, s, OCH_3). ^{13}C NMR (101 MHz, $CDCl_3$) δ 166.24(CO), 154.34(C), 142.56(C), 132.17(C), 132.07(C), 132.04(C), 131.52(C),128.59(CH),128.10(CH) 128.47(CH), 125.26(CH), 113.68(CH), 112.78(CH), 57.88(OCH_3)

Methyl 5-(thiophen-3-yl) benzofuran-2-carboxylate **(5g)** Starting with **3** (0.15 g, 0.598 mmol), Pd (PPh_3) Catalyst (0.035 g, 2.99 mmol), K_3PO_4 (0.13 g, 0.126 mmol), and $C_6H_5B(OH)_2$, (0.0829 g, 0.68mmol).

Yield 70%. Colorless solid, mp146 °C. ^{1}H NMR (400 MHz, $CDCl_3$) δ 7.53 (1H, s, ArH), 7.39(1H, d,j=4, ArH), 7.43(1H, s, ArH), 7.59(1H, d, ArH),7.68(1H, d, j=4, ArH) ,7.85(1H, s, ArH), 3.96 (3H, s, OCH_3) ^{13}C NMR (101 MHz, $CDCl_3$) δ 159.86 (CO), 155.04(C), 145.96(C), 141.88(C), 139.58(C), 132.23(C), 126.87(CH), 126.50(CH), 126.46(CH), 120.32(CH), 120.22(CH), 114.07(CH), 112.55(CH) , 52.42(OCH_3).

Methyl 5-(pyridin-3-yl)benzofuran-2-carboxylate **(5h)** Starting with **3** (0.15 g, 0.598 mmol), $Pd(PPh_3)$ Catalyst (0.035 g, 2.99 mmol), K_3PO_4 (0.13 g, 0.126 mmol), and $C_6H_5B(OH)_2$, (0.0829 g, 0.68mmol). Yield 67% Colorless solid, mp145-149 °C. ^{1}H NMR (400 MHz, $CDCl_3$) δ 8.92(1H, s, ArH), 7.89(1H, s, ArH), 7.71(1H, s, ArH), 7.66(1H, d,j = ArH), 7.59(1H, s, ArH), 8.11(3H, m, ArH), 3.99 (3H, s, OCH_3)**.** ^{13}C NMR (101 MHz, $CDCl_3$) δ160.30(Co), 159.99(C), 150.27(CH), 147.26(CH), 145.90(C), 135.90(CH), 135.21(CH), 134.24(CH), 131.53(CH), 124.52(CH), 122.87(CH), 118.50(CH), 115.49(C), 112.48(CH), 52.01(OCH_3).

Results/Discussion

Chemistry

In the recent research, we employed 5-Bromo salicylaldehyde **(1**), which was first subjected to esterification in accordance with the previously outlined methodology. Compound (**1**) was reacted with methyl chloroacetate **(2**), resulting in the formation of Methyl 6-bromo-1H-indene-2-carboxylate (**3,** 71% yield) (Scheme 1). K_2CO_3 acted as the catalyst in the previously described process, employing Dimethyl formamide (DMF) as a solvent, while the mixture was subjected to reflux for a period of 6 to 8 hours. The derivatives of Compound **3** (**5a**–**5h**) were synthesized through the reaction of (**3**) with a range of acids (**4**), employing $Pd(PPh_3)_4$ for Suzuki coupling at a temperature of 90 °C. In this work, we executed C-C couplings utilizing 1,4-dioxane(solvent/water), maintaining ratio (6:1); the synthesized benzofuran derivatives (**5a**–**5h**) were acquired with yields varying from 60.9% to 89.2% (Table 1) (Scheme 1). The elevated solubility of phenyl boronic acid in 1,4-dioxane/water may be the underlying factor contributing to the increased yield. The noteworthy aspects include highest/lowest yield of thiophene analogues, which are influenced by electron withdrawing and electron donating groups effects. The compound (**5a**) demonstrated a peak yield of 78% in conjunction with the electron-donating group. In contrast, (**5d)** exhibited a minimum yield of 63%, attributable to the presence of an electron-withdrawing substitution within the benzofuran analogues (Schemes-1).

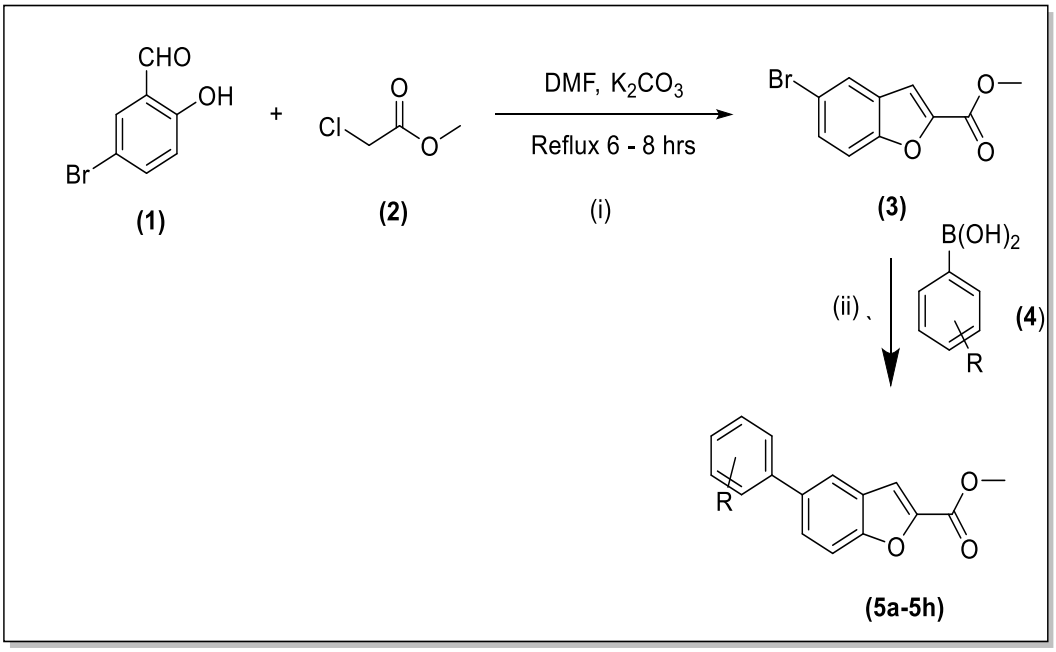

Schemes-1: Synthesis of phenylbenzofuran-2-carboxylate derivatives (5a-5f) *Vi a* Suzuki cross coupling reactions.

Conditions (i) Bromosalicylaldehyde (2 g, 0.016mol), DMF (30 ml), methylchloroacetate (1.91 g, 0.0176 mol), base K_2CO_3 (2.43 g, 0.0176 mol),85 °C. (ii) 6 mL of 1,4-dioxane/water, 3 (0.15 g, 0.46 mmol), substituted phenyl boronic acid **4** (1.1 eq), 5 mol% $Pd(PPh_3)_4$, 2 eq. K_3PO_4, 16 h reflux at 90 °C.

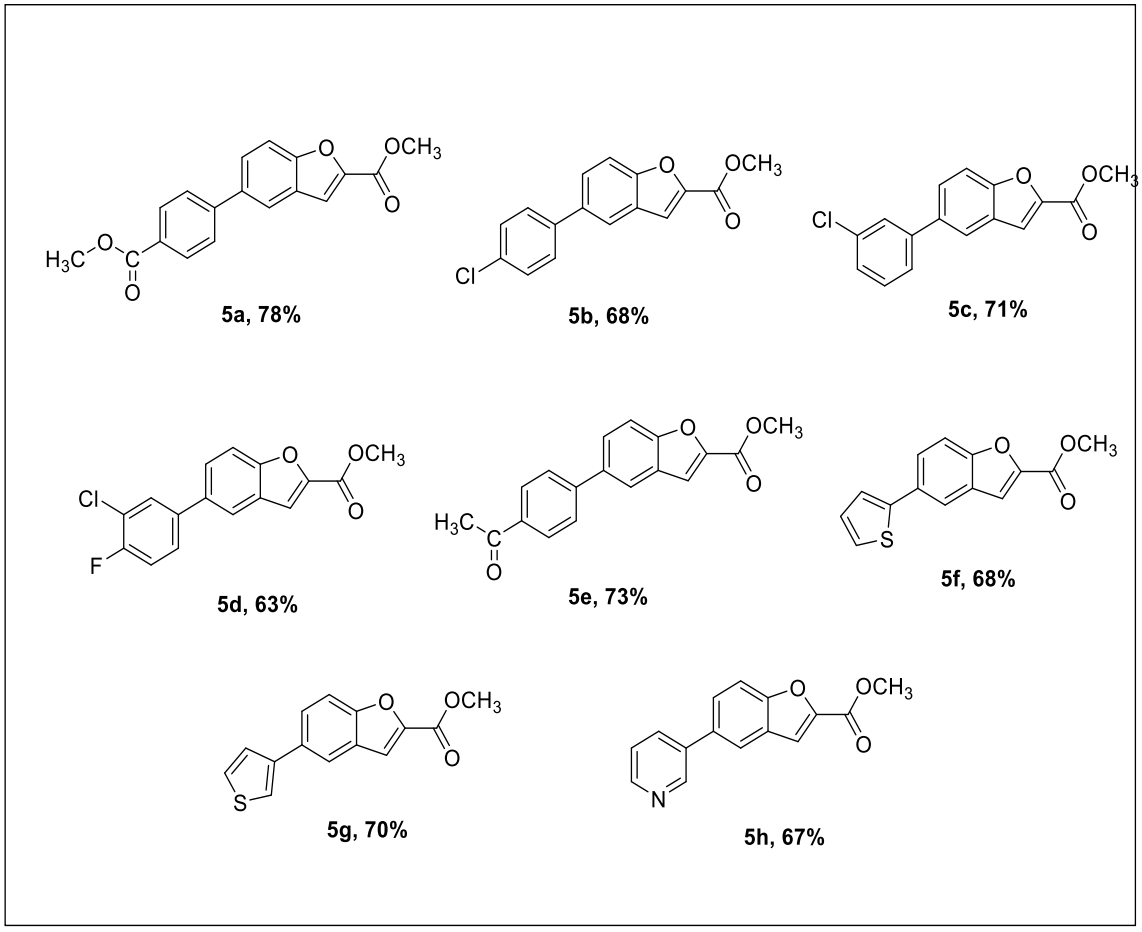

Fig. 1: Percentage yield of phenylbenzofuran-2-carboxylate derivatives (5a-5f) synthesized through Suzuki cross coupling reactions.

Spectral interpretation of compounds **(5a–5h)**

There were studied factors affecting the optimization of reactions. The effect of solvent on the coupling reactions between 3 and different aryl boronic acids under thermal conditions at 85–90 °C was evaluated. *Methyl 5-(4-(methoxycarbonyl) phenyl) benzofuran-2-carboxylate* (5a) was obtained in good yield when 3 was coupled with phenylboronic ester in 4:1 toluene/water in the presence of 5 mol% of the Pd (0) catalyst using K_3PO_4 as base. The 1H-NMR spectrum of product (5a) gave a multiplet signals for the benzofuran ring protons in the δ 7.52–7.68 ppm region. The aryl protons present also showed singlets at δ 7.88 ppm and a doublet at δ 8.10 ppm, respectively. Moreover, the presence of two methoxy groups at aryl and benzofuran ring was confirmed by appearance of two singlets at δ 3.93 and δ 3.98 ppm. The ^{13}CNMR spectrum also supported the carbon framework of synthesized compound 5a. All carbons displayed signals in spectrum and two carbonyl groups showed signals δ 166.6 and δ 155.8 certified the presence of benzofuran based ester. Signals indicating the formation of benzofuran appeared at δ 112.64, δ 114.04, δ 121.01, δ 130.07, δ 130.67, δ 136.15, δ 146.11, and δ 155.31. The carbons of aryl group attached with benzofuran ring depicted their signals at δ 125.55, δ 127.53, δ 127.50, δ 128.89, δ 134.07 and δ 142.68. Two methoxy substituents depicted signals on the right side of spectrum at δ 52.16 and δ 52.49.

Moreover, the smooth coupling of compound 3 with 4-chlorophenylboronic acid under heating conditions gave *Methyl 5-(4-chlorophenyl) benzofuran-2-carboxylate*(5b) in excellent yield. Its 1H-NMR spectrum revealed two doublets at δ 7.40

ppm and δ 7.50 ppm assigned to 4 H at positions 2 and 3 of the aryl ring, respectively. In addition, the presence of methoxy groups at benzofuran ring also confirmed by appearance of singlet at δ 3.98 ppm. Carbons of 5b displayed ^{13}CNMR signals in spectrum in which carbonyl group showed signal at δ 159.93 confirming the presence of benzofuran ester. Signals demonstrating the formation of benzofuran appeared at δ 112.73, δ 113.85, δ 114.15, δ 121.44, δ 130.67, δ 136.34, δ 146.20, and δ 155.58. The carbons of aryl group attached with benzofuran ring in the result of Suzuki coupling depicted their signals at δ 125.55 δ 127.20, δ 127.50, δ 127.53, δ 134.71, and δ 142.68. The methoxy substituents showed signals on the right side of spectrum at δ 52.4.

Methyl 5-(3-chlorophenyl) benzofuran-2-carboxylate **(5c)** was synthesized by coupling compound 3 with 3-chlorophenylboronic acid under at prescribed conditions. The 1H-NMR spectrum of this product gave a 3H singlet for the methoxy group in the δ 3.96 ppm region and a singlet for the phenyl ring protons at position 2 in the δ 7.82 ppm region. Moreover, two doublet signals for 4 and 6 position and one triplet for 5 position of aryl group showed signals at 7.37,7.45 and 7.33 ppm. In spectrum of 5c the carbons displayed ^{13}CNMR signals in which carbonyl group showed signal at δ 159.81 proving the presence of benzofuran ester. Signals demonstrating the formation of benzofuran appeared at δ 112.68, δ 114.05, δ 121.22, δ 130.07, δ 130.67 δ 136.15, δ 146.15, and δ 155.43. The carbons of aryl group attached with benzofuran ring in the result of Suzuki coupling depicted their signals at δ 125.55 δ 127.29, δ 127.50, δ 127.53, δ 134.71, and δ 142.68. The methoxy substituents showed signals on the right side of spectrum at δ 52.48.

Compound 5d was synthesized by coupling 3 with 3-chloro-4-fluro phenylboronic acid at heating condition. The 1H-NMR spectrum of this product gave a 3H singlet for the methoxy group in the δ 3.98 ppm region. and a multiplet for the phenyl ring protons in the δ 7.2–7.4 ppm region. The aryl 1H present at positions 2 showed a singlet at δ 7.78 ppm whenever 2H at position 5 and 6 of phenyl group showed doublet and mutiplet at δ 7.24ppm and δ 7.42ppm, respectively. The carbons of 5d showed ^{13}CNMR signals in spectrum in which carbonyl group showed signal at δ 159.77 proving the presence of benzofuran ester. Signals demonstrating the formation of benzofuran appeared at δ 112.74, δ 113.95, δ 127.05, δ 116.79, δ 127.15 δ 135.37, δ 146.25, and δ 153.34. The carbons of aryl group attached with benzofuran ring in the result of Suzuki coupling depicted their signals at δ 117.00 δ 121.11, δ 127.53, δ 129.49, δ 138.15, and δ 156.40. The methoxy substituents showed signals on the right side of spectrum at δ 52.46. By reacting 3 and 3-acetyl phenyl boronic acid the compound 5e was synthesized. The 1H-NMR spectrum of this product gave a 3H singlet for the methyl group in the δ 2.64 ppm region and two doublets at δ 7.66 ad δ 7.35ppm. The methoxy group of benzofuran ring showed a singlet in δ 3.98 ppm region. In ^{13}CNMR spectrum all carbons of 5e exhibited signals in which carbonyl group showed signal at δ 159.77 certifying the presence of benzofuran based ester. Signals demonstrating the formation of benzofuran appeared at δ 112.69, δ 114.03, δ 121.30, δ 127.10, δ 131.94 δ 136.51, δ 146.18, and δ 159.80. The carbons of aryl group attached with benzofuran ring in the result of Suzuki coupling depicted their signals at δ 127.40, δ 127.36, δ 127.54, δ 129.13, δ 137.67, and δ 141.37. The methoxy substituents showed signals on the right side of spectrum at δ 52.48. Carbonyl group of phenyl ring showed signal at δ 159.77 and signal for methyl group was shown at δ 26.6. The compound 5f was synthesized by coupling 3 and 2-thiophene boronic acid. Its 1H-NMR spectrum revealed two doublets at δ 7.46 and δ 7.48 ppm due to the protons at the 3 and 5 positions in the thiophene ring, respectively. Moreover, one triplet appeared at δ 7.54 ppm due to the protons at positions 4 in the thiophene, respectively. Moreover, a singlet appeared at δ 3.55 ppm elaborating the presence of methoxy groups at benzofuran ring. The carbons of 5f showed ^{13}CNMR signals in spectrum in which carbonyl group showed signal at δ 166.24 certifying the presence of benzofuran ester. Signals demonstrating the formation of benzofuran appeared at δ 112.78, δ 113.68, δ 125.26, δ 128.47, δ 132.07, δ 132.17, δ 142.56, and δ 154.34. The carbons of thiophene ring attached with benzofuran ring in the result of Suzuki coupling depicted their signals at δ 128.10, δ 128.59, δ 131.52and δ 132.04. Coupling of compound 3 with 3-thiophene phenylboronic acid under heating conditions gave *Methyl 5-(thiophene-3-yl) benzofuran-2-carboxylate*(5g). Its 1H-NMR spectrum revealed two doublets at δ 7.39 and δ 7.41 ppm due to the protons at the 4 and 5 positions in the thiophene ring, respectively. Moreover, one singlet appeared at δ 7.85 ppm due to the proton at positions 2 in the thiophene, respectively. In addition, the presence of methoxy groups at benzofuran ring also confirmed by appearance of singlet at δ 3.98 ppm. ^{13}CNMR signals in spectrum of 5f are elaborated in which carbonyl group showed signal at δ 159.86 certifying the presence of benzofuran ester. Signals demonstrating the formation of benzofuran appeared at δ 112.5, δ 114.07, δ 120.22, δ 120.32, δ 132.33, δ 141.88, δ 145.96, and δ 155.04. The carbons of thiophene ring

attached with benzofuran ring in the result of Suzuki coupling depicted their signals at δ 126.48, δ 126.50, δ 126.87 and δ 139.58. The most efficient coupling of compound 3 with 3-pyridinyl boronic acid produced *Methyl 5-(pyridin-3-yl) benzofuran-2-carboxylate* (5h) in excellent yield after heating for 12 h. The 1H-NMR spectrum of compound 5h gave a 3H singlet for the methoxy group in the δ 3.89 ppm region and a multiplet for the pyridinyl ring protons in the δ 8.08–8.11 ppm region. All carbons of 5h displayed ^{13}CNMR signals in spectrum in which carbonyl group showed signal at δ 160.33 certifying the presence of benzofuran ester. Signals demonstrating the formation of benzofuran appeared at δ 112.48, δ 115.49, δ 118.50, δ 122.87, δ 131.53 δ 135.90, δ 145.90, and δ 159.99. The carbons of aryl group attached with benzofuran ring in the result of Suzuki coupling depicted their signals at δ 124.52, δ 134.24, δ 135.21, δ 147.26, and δ 150.27. The methoxy substituents showed signals on the right side of spectrum at δ 52.1.

Pharmacological aspects of synthesized compounds **(5a-5h)**

α-Glucosidase Inhibitiory study

All synthesized derivatives (**5a-5h**) underwent screening for α-Glucosidase inhibitory potential utilizing the Saccharomyces cerevisiae, EC3.2.1.20 (α-Glucosidase). The synthesized compounds (**5a-5h**) demonstrated significant inhibitory potential, with IC_{50} values ranging from 47.3 ± 2.30 to 73.1 ± 1.16 µM for α-glucosidase, in comparison to acarbose (reference drug), which has an IC_{50} value of 375.82 ± 1.76µM. Among the synthesized compounds, it was observed that the molecule **5a** (IC_{50}= 47.3±2.30µM) containing the MeOCO group demonstrated the highest potency as an inhibitor.

Table 1: α-Glucosidase inhibition data of compounds (**5a–5h**)

Compd.	Urease Inhibition IC_{50}(µM)	α-Glucosidase Inhibition IC_{50}(µM)
5a	**82.37 ± 2.13**	**47.3±2.30**
5b	**66.83 ± 1.66**	-
5c	**73.40 ± 2.35**	---
5d	------	**49.2±1.31**
5e	**68.28±1.16**	**445.3±2.32**
5f	-------	----
5g	**71.25±1.41**	**73.1±1.16**
5h	-------	-
Thiourea	**21.37±1.76**	-
Acarbose	-	**375.82±1.76**

The compound (**5a)** demonstrates a potency nearly eight times more effective than that of the standard acarbose. It was noted that presence of electron-withdrawing substitution, such as halogens, resulted in a slight reduction of inhibitory activity. Consequently, compound **5d** (IC_{50}= 49.2±1.31µM) exhibited a reduction in inhibitory activity due to the presence of two halogen substituents, fluoro and chloro [36]. The compound **5e** (IC_{50}=445.3±2.32µM) exhibited reduced activity compared to the standard drug acarbose, attributed to the presence of the CH_3CO group, which is characterized as electron withdrawing. The structure-activity relationship has been conducted, primarily influenced by the type, number, position, and effect of electron donating/withdrawing substitution [37].

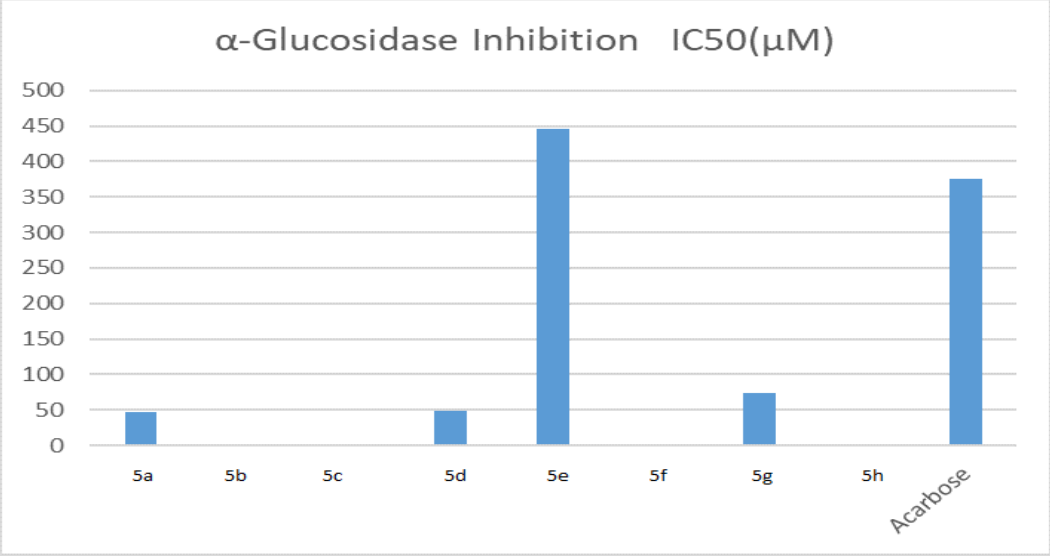

Fig. 2: α-Glucosidase inhibition data of compounds (**5a–5h).**

Urease Inhibition study

The compound **(5b**) demonstrates a good potency nearly than that of the standard thiourea. It was noted that the presence of electron-withdrawing halogens substitution, resulted in a slight reduction of inhibitory activity. Consequently, compound (**5d)** exhibited no activity due to both halogens at meta and para positions [38]. The compound **5e** (IC_{50}=68.28±1.16µM) exhibited relatively moderate activity compared to the standard thiourea, attributed to the presence of the CH_3CO group, which is characterized as electron withdrawing. The structure-activity relationship has been conducted, primarily influenced by the type, number, position, and donating/withdrawing substitution effects.

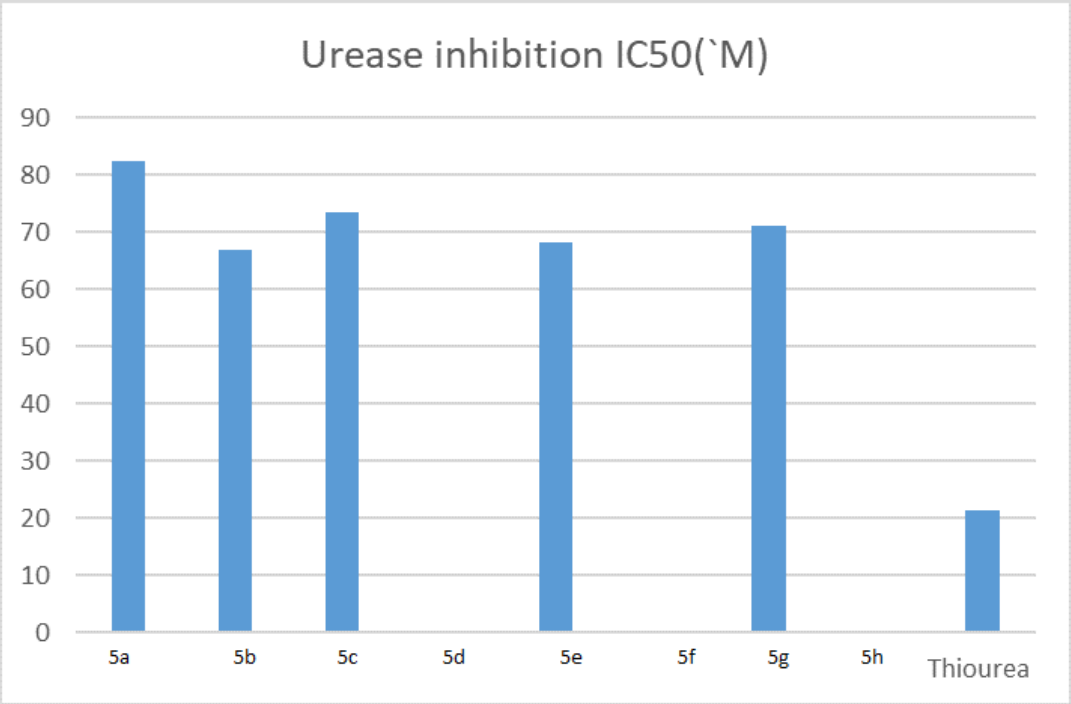

Fig. 3: Anti-urease inhibition data of compounds **(5a–5h)**.

Hemolytic activities of compounds **(5a-5h)**

The benzofuran-based analogues (**5a−5h**) were additionally evaluated for hemolytic assay. Hemolysis percentage was analyzed, and the results are presented in Fig 4. The lowest toxicity was observed for molecule **5g** (8.1%), which exhibited minimal interaction with RBCs cell membrane in comparison to the ABTS (95.9%) hemolysis (standard). The analysis revealed that derivative **5f** was identified as the most toxic compound, exhibiting a hemolysis rate of 31.9%. In comparison, the other derivatives displayed varying levels of hemolytic activity: **5a** at 27.7%, 5b at 31%, 5h at 9.5%, 5d at 29.1%, and 5e at 30.1%, indicating moderate to low hemolytic activity across the board. SAR was examined based on the substituents on phenyl functional moiety substitution of substituted benzofuran derivatives (**5a-5h**) to gather comprehensive information regarding the hemolytic activities of the synthesized derivatives. Structural substitution and activities of synthesized analogs under examination indicates that the incorporation of an electron-donating substituents typically results in lower toxicity. Compounds **5e, 5g,** and **5h**, exhibiting hemolytic activities of 29%, 8.1%, and 9.5% respectively, demonstrate lower toxicity. In contrast, compounds with electron-withdrawing substituents on the phenyl ring, namely **5b, 5c,** and **5d,** show hemolytic activities of 31%, 31.8%, and 30%, respectively, indicating higher toxicity. The findings indicate that the characteristics and placement of the functional groups considerably influence the hemolytic potential of the synthesized derivatives [28].

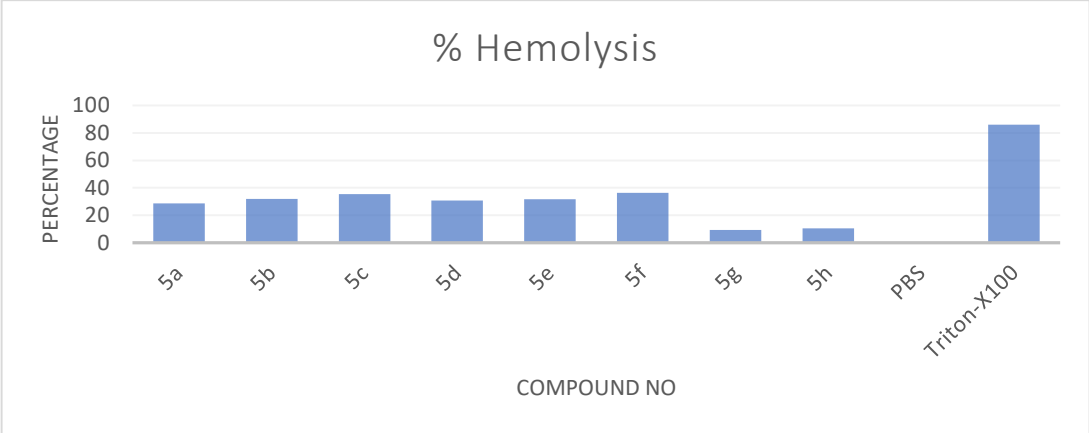

Fig. 4: Hemolytic activity of compounds (**5a– 5h**)

Table-2: Antibacterial (Inhibition Zone in mm) and Hemolytic data of compounds (**5a–5h**).

Compound	*E. coli*	*B. Subtilis*	%age hemolytic activity
5a	**2**	**2**	**27.7**
5b	**5**	**3**	**31**
5c	**2**	**2**	**31.8**
5d	**2**	**4**	**30**
5e	**3**	**2**	**29**
5f	**2**	**2**	**32**
5g	**9**	**3**	**8.1**
5h	**2**	**2**	**9.5**
Ciprofloxacin	**30**	**27**	---------
ABTS	------	------	**95.5%**

Antibacterial activities of compounds **(5a-5h)**

The assessment of in vitro antibacterial efficacy of synthesized analogs (**5a-5h**) was conducted against two bacterial strains, B. subtilis (Gram-positive) and Gram-negative bacteria (Escherichia coli). The findings presented in Table 3 demonstrate that all eight compounds (**5a-5h**) displayed moderate to good antibacterial activities in comparison to the standard drug ciprofloxacin. Notably, compound **(5b**) exhibited significant efficacy against E. coli, demonstrating a zone of inhibition measuring 5mm in contrast to the standard drug ciprofloxacin, which recorded an inhibition value of 27 mm. Furthermore, compound (**5g**) exhibited the highest activity 9mm against E. coli when compared to all the synthesized compounds. Moreover, Compound **(5d**) demonstrated a moderate level of antibacterial activity, measuring 4 mm when tested against Gram-positive bacteria (B. subtilis). All other derivatives (i.e., **5a, 5c, 5e, 5f, 5h**) exhibited reduced inhibitory activity against Escherichia coli and Gram-positive bacteria (B. subtilis) when ciprofloxacin was uti lized as the reference drug. Table 2 illustrates that the presence of a chloro group at the para position within a molecule enhances antibacterial activities, as observed in the synthesized molecule (**5b**). In contrast, substitution at the meta position leads to a reduction in antibacterial activity, as demonstrated by **(5c**). The synthesized compound (**5d**) exhibited slightly enhanced activity against the Gram-positive Bacteria B. subtilis, attributable to the presence of two halogen groups attached. The SAR studies elucidate the interplay of factors such as the nature, position, and diversity of substituents, which collectively define the antibacterial activities of various synthesized molecules (Fig 5) [39].

Molecular Docking

The docking scores of the synthesized compounds (**5a – 5h)** against various targets indicate their potential as effective enzyme inhibitors, with the majority exhibiting KI values below 3 µM, with a few exceptions noted. Compound **5e** KI value through docking predicted is 1.08 µM lowest among all target compounds and invitro α-glucosidase inhibition is comparable with the standard Acarbose. Similarly compound **5b** and **5d** also show low KI values 1.66 and 1.24 µM respectively and also show significant invitro biological activities. Compounds **5a, 5c**, and **5h** demonstrate a strong affinity through hydrogen bonding and electrostatic interactions with the active site of ligand residues within chains 50 to 400, specifically residues of active site of receptor protein isomaltase PDB ID: 3A47 PHE159, GLY160, GLY161, LYS156, TYR158, and PHE178 (see **SI Table 1**). For a visual representation, referring to the docking Fig 6 of ligand 3 is represented in Fig 4, while detailed docking score of all target compounds can be found in Table 3. Based on the docking results, the synthesized analogs were subjected to *in vitro* enzymatic studies targeting urease and α-Glucosidase inhibition.

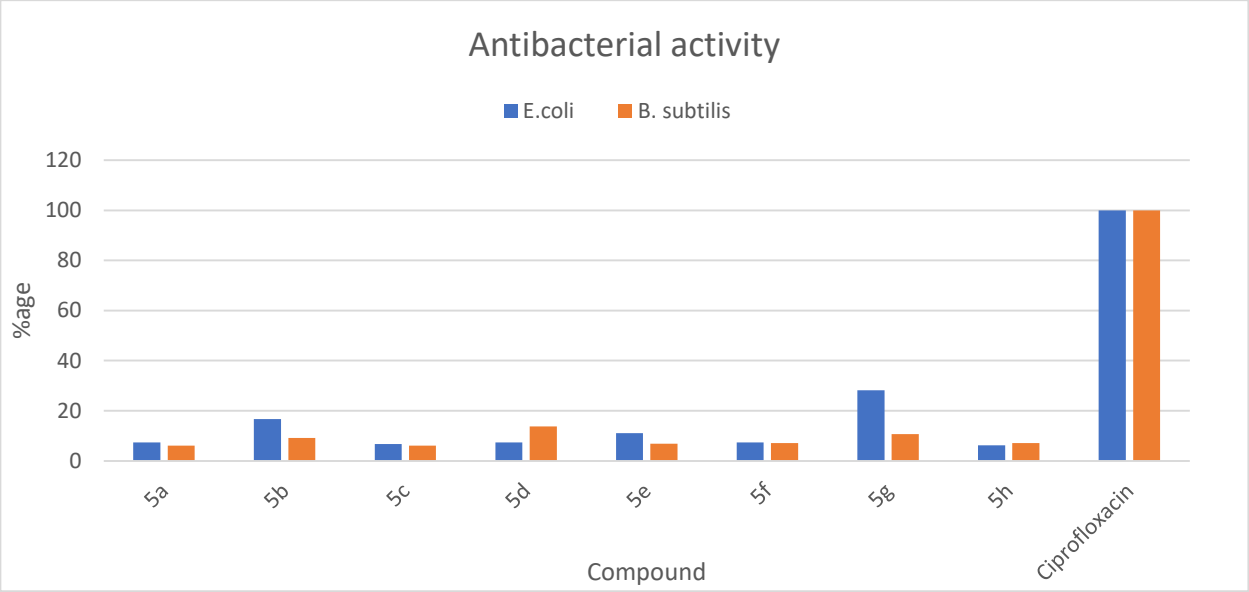

Fig. 5: Antibacterial activity of compounds (**5a-5h**).

Table-3: Docking Score of Ligand (5a– 5h) with receptor molecule.

Ligand	Ligand optimization kJ/mol	Binding Energy:	kI : uM	Intermolecular Energy	Internal Energy	Torsional Energy	Unbound Extended Energy-	Ref RMS:
5a	**324.411**	**-6.7**	**12.17**	**-8.2**	**-0.67**	**1.49**	**0.67**	**27.41**
5b	**201.321**	**-7.88**	**1.66**	**-8.78**	**-0.49**	**0.89**	**-0.49**	**28.67**
5c	**189.965**	**-6.46**	**18.24**	**-7.36**	**-0.59**	**0.89**	**-0.59**	**22.21**
5d	**264.074**	**-8.06**	**1.24**	**-8.95**	**-0.5**	**0.89**	**-0.5**	**31.08**
5e	**286.996**	**-8.14**	**1.08**	**-9.33**	**-0.69**	**1.19**	**-0.69**	**35.24**
5f	**157.384**	**-7.57**	**2.83**	**-8.46**	**-0.53**	**0.89**	**-0.53**	**35.85**
5g	**145.108**	**-7.33**	**4.27**	**-8.22**	**-0.51**	**0.89**	**-0.51**	**40.43**
5h	**278.825**	**-4.86**	**274.18**	**-5.75**	**-0.44**	**0.89**	**-0.44**	**0.0**

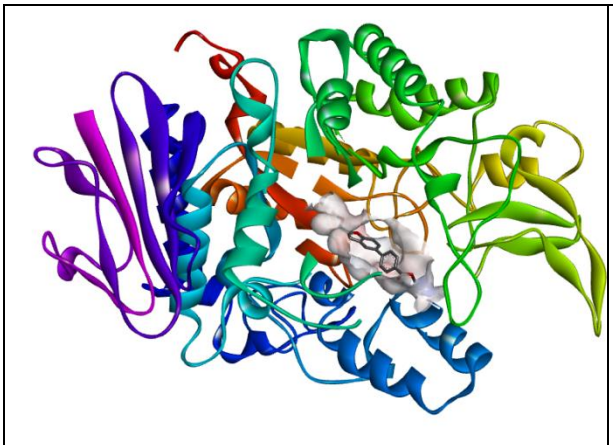

(A): Interaction of ligand (**5c**) inside the active pocket of receptor PDB ID: 3A47

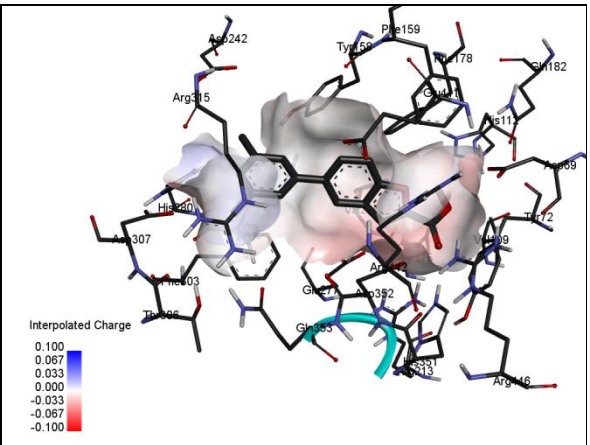

(B): 3D view of ligand (**5c**) interaction inside the active pocket of receptor PDB ID: 3A47

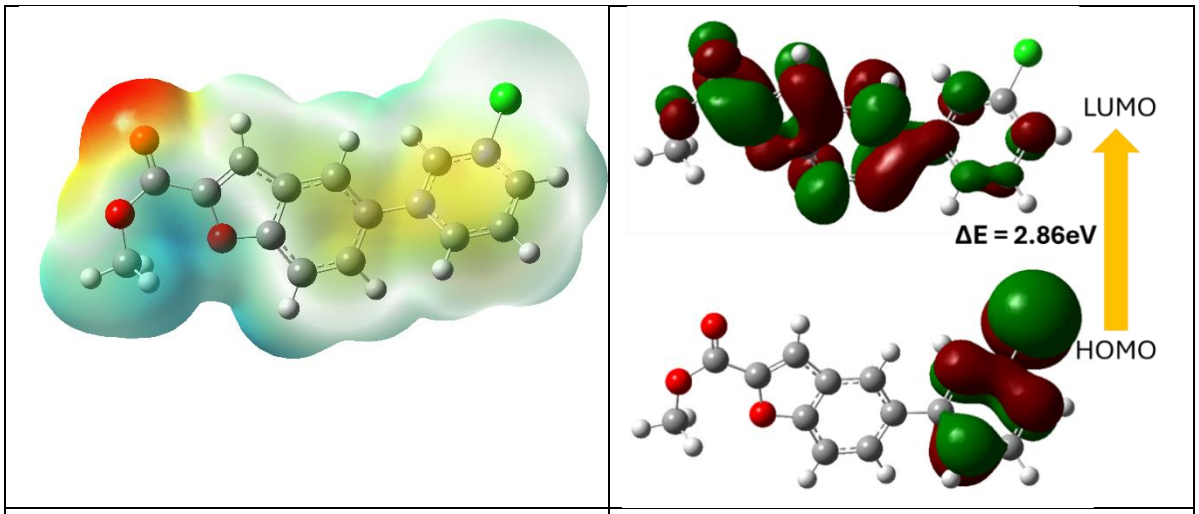

(C) Molecular electrostatic potential on molecule (5c).

(D): HOMO – LUMO gap of ligand (**5c**)

Fig 6: Molecular docking of target molecule (5c) and its HOMO-LUMO energy gap.

Table-4: DFT calculations data using B3LYP method with basis set 6-31G(d,p).

Compound	HOMO (eV)	LUMO (eV)	ΔE (eV)	Energy (Hartree)	Dipole moment (Deby)	Pearson's absolute hardness η(eV)	Mulliken electronegativity χ(eV)	electrophilicity indices, ω (eV)
5a	-6.536	-1.967	4.57	-1070.80	3.81	2.2845	4.2515	3.956063
5b	-6.409	-1.922	4.49	-1302.48	2.58	2.2435	4.1655	3.867036
5c	-8.102	-5.239	2.86	-1303.04	3.43	1.4315	6.6705	15.54159
5d	-6.478	-1.935	4.54	-1401.74	1.76	2.2715	4.2065	3.894925
5e	-6.524	-2.034	4.49	-995.55	5.44	2.245	4.279	4.077916
5f	-8.256	-5.204	3.05	-1163.36	4.11	1.526	6.73	14.8404
5g	-8.158	-5.180	2.98	-1163.37	2.12	1.489	6.669	14.93471
5h	-8.829	-5.232	3.59	-858.65	2.73	1.7985	7.0305	13.74143

Structural features of synthesized compounds

HOMO and LUMO Analysis

Frontier orbitals, referred to as HOMO (highest occupied molecular orbital) and LUMO (lowest unoccupied molecular orbital), serve as substantial indicators of electrical features within dominion of quantum chemistry. The shift from HOMO to LUMO is characterized by the phenomenon of light absorption. HOMO orbitals signify the entities that donate electrons, whereas LUMO orbitals denote those that accept electrons. The surfaces of the frontier orbitals pertaining to the compound under consideration are illustrated in the accompanying Fig. The existence of electron clouds surrounding the oxygen atoms and the benzofuran ring indicates their participation in the charge transfer property. The hues of red and green signify the affirmative and negative aspects of the molecular orbital wave function, correspondingly. The presence of abundant electron clouds in π atomic orbitals facilitates the electronic transition from HOMO to LUMO, primarily through electronic π-π* transitions occurring within the molecules. All compounds exhibit a HOMO-LUMO energy gap that suggests their potential as biologically active. entities i.e. Compound 5c, 5f and 5g show minimum HOMO – LUMO gap 2.86, 3.05, 2.98 eV respectively, which also predict them biologically active compounds (Table 2, Fig 1 - 3 Supplementary Data).

Mulliken Charge Analysis elucidates the distribution of electronic charges among the atoms of a molecule, thereby highlighting the electrophilic and nucleophilic centers present within the molecular structure. The illustration depicts the Mulliken charge values of the constituent atoms of the molecule under examination, with high electron density transitioning to positive charge density, represented by a gradient from red to brown to black to green to light green on the respective atoms. Every hydrogen atom is imbued with a positive charge. The atom exhibiting the highest positive charge within the molecule is the carbonyl carbon, or the carbon atom adjacent to the oxygen atom in the furan ring, which characterizes them as electrophilic centers. Concurrently, the distribution of electron density predominantly occurs on oxygen atoms, attributable to their inherent electronegativity.

In summary, the electronic cloud is situated on aromatic rings.

The delineation of electrostatic potential, as informed by molecular electrostatic potential (MEP), renders it an essential instrument for discerning both nucleophilic and electrophilic interactions. Regions characterized by negative electrostatic potential are more conducive to electrophilic attack, whereas regions with positive electrostatic potential are linked to nucleophilic attack. A representation of the electrostatic potential ranges in MEP is presented in a colour-coded format. In the target molecules, the bluish-green and red hues signify the positive and negative electrostatic regions, respectively, while the yellow hue indicates the area of low electron density. The sequence red, yellow, green, light blue, and blue represents the progression in which the positive electrostatic potential on the molecular surface escalates. Illustration 1.

Electrophilicity and Hardness

In 2002, Domingo et al. established a singular scale of electrophilicity, which emerged from an extensive investigation into the electrophilic properties of various prevalent reagents employed in experimental Diels–Alder (DA) reactions41. This classification system categorizes organic molecules into three distinct groups: with $\omega \geq 1.5$ eV(strong electrophiles), with $0.8 \leq \omega < 1.5$ eV (moderate electrophiles), and with $\omega < 0.8$ eV (marginal electrophiles), while super electrophiles are identified for species where $\omega \geq 4.0$ eV (refer to Table 1). Only robust electrophiles demonstrate efficacy in experimental settings. The rigidity of the molecule signifies its level of resistance to alterations in the electron cloud during chemical interactions. Soft systems exhibit greater size and polarizability, whereas hard systems are characterized by their compactness and reduced polarizability. Based on DFT calculations, the target molecules are classified within the category of soft molecules (Table-1).

Conclusion

The current study demonstrates that target molecules were synthesized with yields ranging from 55% to 80% through the Suzuki-Miyura reaction. The structures were validated through NMR analysis, which also confirms the successful synthesis. Additional structural characteristics of target compounds assessed via DFT studies and molecular docking. Significant interaction between the target compounds and the proteins has been validated through comprehensive structural computational insights. Based on computational predictors, in vitro studies were conducted on these molecules, including assessments of α-glucosidase activity, anti-urease properties, hemolytic effects, and antibacterial efficacy. The studies identified compounds (**5b**, **5c**, **5e**, and **5g**) as potential urease inhibitors and compounds (**5a**, **5d**, and **5g**) as potential α-glucosidase inhibitors. The findings of our study indicate that these compounds warrant further investigation as potential new medication candidates due to their significant inhibitory action against both anti-diabetic and anti-urease activity.

Acknowledgment:

The present data is part of the PhD research work of Lal Khan. The authors gratefully acknowledge the PCSIR (Ministry of Science and Technology), through the data repository of the scientific instrumentation development program initiated in 2021.

References

1. Mekala, K.C. and A.G. Bertoni, *Epidemiology of diabetes mellitus*, in *Transplantation, bioengineering, and regeneration of the endocrine pancreas*. 2020, Elsevier. p. 49-58, https://doi.org/10.1016/B978-0-12-814833-4.00004-6.
2. Dórea, J.V.F., W.R. Borges, and P.R.B. Ferracioli, *The Main Diseases Related to Type 2 Diabetes Mellitus: A Scoping Review.* Scientia. Technology, Science and Society, 2024. **1**(2): p. 17-27, https://doi.org/10.59324/stss.2024.1(2).02.
3. Ahmed, N. and L.A. Sechi, *Helicobacter pylori and gastroduodenal pathology: new threats of the old friend.* Annals of clinical microbiology and antimicrobials, 2005. **4**: p. 1-10, https://doi.org/10.1186/1476-0711-4-1.
4. Waskito, L.A., et al., *The role of non-Helicobacter pylori bacteria in the pathogenesis of gastroduodenal diseases.* 2022. **14**(1): p. 1-19, https://doi.org/10.1186/s13099-022-00494-0.
5. Popovic-Djordjevic, J.B., I.I. Jevtic, and T.P. Stanojkovic, *Antidiabetics: Structural diversity of molecules with a common aim.* Current medicinal chemistry, 2018. **25**(18): p. 2140-2165, https://doi.org/10.2174/0929867325666171205145309.
6. Cai, W., et al., *Rational design of α-glucosidase activated near-infrared fluorescent probe and its applications in diagnosis and treatment of diabetes.* Sensors and Actuators B: Chemical, 2024. **400**: p. 134878, https://doi.org/10.1016/j.snb.2023.134878.

7. Kim, Y., et al., *Glycosidase-targeting small molecules for biological and therapeutic applications.* Chemical Society Reviews, 2023. **2023**(20): p. 1-35, https://doi.org/10.1039/D3CS00032J.
8. Lu, H., et al., *Alpha-Glucosidase inhibitory peptides: Sources, preparations, identifications, and action mechanisms.* Nutrients, 2023. **15**(19): p. 42-67, https://doi.org/10.3390/nu15194267.
9. Paunica, I., et al., *Diabetes mellitus and associated complications in the digestive tract.* Journal of Mind and Medical Sciences, 2024. **11**(2): p. 351-362, https://doi.org/10.22543/2392-7674.1567.
10. Pires, L., et al., *The Role of Gut Microbiota in the Etiopathogenesis of Multiple Chronic Diseases.* Antibiotics, 2024. **13**(5): p. 392, https://doi.org/10.3390/antibiotics13050392.
11. Fatima, N., et al., *Approachable Synthetic Methodologies for Second-Generation β-Lactamase Inhibitors: A Review.* Pharmaceuticals, 2024. **17**(9): p. 1-62, https://doi.org/10.3390/ph17091108.
12. Paliya, B., et al., *The genus Usnea: A potent phytomedicine with multifarious ethnobotany, phytochemistry and pharmacology.* RSC advances, 2016. **6**(26): p. 21672-21696, https://doi.org/10.1039/C5RA24205C.
13. Kanwal, A., et al., *Synthesis of anti-depressant molecules via metal-catalyzed reactions: a review.* RSC advances, 2024. **14**(10): p. 6948-6971, https://doi.org/10.1039/D3RA06391G.
14. Radadiya, A. and A. Shah, *Bioactive benzofuran derivatives: An insight on lead developments, radioligands and advances of the last decade.* European journal of medicinal chemistry, 2015. **97**: p. 356-376, https://doi.org/10.1016/j.ejmech.2015.01.021.
15. Kwiecień, H. and A. Wodnicka, *Five-membered ring systems: furans and benzofurans.* Progress in Heterocyclic Chemistry, 2020. **31**: p. 281-323, https://doi.org/10.1016/B978-0-12-819962-6.00007-5.
16. 16. Khanam, H., *Bioactive Benzofuran derivatives: A review.* European journal of medicinal chemistry, 2015. **97**: p. 483-504, https://doi.org/10.1016/j.ejmech.2014.11.039.
17. Khalil, N.S., *Efficient synthesis of novel 1, 2, 4-triazole fused acyclic and 21–28 membered macrocyclic and/or lariat macrocyclic oxaazathia crown compounds with potential antimicrobial activity.* European journal of medicinal chemistry, 2010. **45**(11): p. 5265-5277, https://doi.org/10.1016/j.ejmech.2010.08.046.
18. Venkatesh, T., et al., *Synthesis of some benzofuran derivatives containing pyrimidine moiety as potent antimicrobial agents.* Iranian Journal of Pharmaceutical Research: IJPR, 2018. **17**(1): p. 75-86, https://pmc.ncbi.nlm.nih.gov/articles/PMC5937079/.
19. Deghady, A.M., et al., *Density functional theory and molecular docking investigations of the chemical and antibacterial activities for 1-(4-Hydroxyphenyl)-3-phenylprop-2-en-1-one.* Molecules, 2021. **26**(12): p. 1-13, https://doi.org/10.3390/molecules26123631.
20. Hertwig, R.H. and W. Koch, *On the parameterization of the local correlation functional. What is Becke-3-LYP?* Chemical Physics Letters, 1997. **268**(5-6): p. 345-351, https://doi.org/10.1016/S0009-2614(97)00207-8.
21. Raghavachari, K., *Perspective on "Density functional thermochemistry. III. The role of exact exchange" Becke AD (1993) J Chem Phys 98: 5648–52.* Theoretical Chemistry Accounts, 2000. **103**: p. 361-363, https://doi.org/10.1007/s002149900065.
22. El-Shamy, N.T., et al., *DFT, ADMET and Molecular Docking Investigations for the Antimicrobial Activity of 6, 6′-Diamino-1, 1′, 3, 3′-tetramethyl-5, 5′-(4-chlorobenzylidene) bis [pyrimidine-2, 4 (1H, 3H)-dione].* Molecules, 2022. **27**(3): p. 1-17, https://doi.org/10.3390/molecules27030620.
23. Khire, S.S., N. Sahu, and S.R. Gadre, *MTASpec software for calculating the vibrational IR and Raman spectra of large molecules at ab initio level.* Computer Physics Communications, 2022. **270**: p. 108175, https://doi.org/10.1016/j.cpc.2021.108175.
24. Panicker, C.Y., et al., *FT-IR, NBO, HOMO–LUMO, MEP analysis and molecular docking study of Methyl N-({[2-(2-methoxyacetamido)-4-(phenylsulfanyl) phenyl] amino}[(methoxycarbonyl) imino] methyl) carbamate.* Spectrochimica Acta Part A: Molecular and Biomolecular Spectroscopy, 2015. **148**: p. 29-42, https://doi.org/10.1016/j.saa.2015.03.064.
25. Mani, N., et al., *Potential energy surface, effect of solvents in molecular level, experimental spectra (FTIR, Raman, UV–visible & NMR), electronic, and dynamics simulation of isobavachalcone–Anti tuberculosis agent.* Journal of Molecular Liquids, 2023. **392**: p. 1-16, https://doi.org/10.1016/j.molliq.2023.123465.
26. Ballante, F., et al., *Structure-based virtual screening for ligands of G protein–coupled receptors: what can molecular docking do for you?* Pharmacological Reviews, 2021. **73**(4): p. 1698-1736, https://doi.org/10.1124/pharmrev.120.000246.
27. Kumar, S., et al., *In-silico identification of small molecule benzofuran-1, 2, 3-triazole hybrids as potential inhibitors targeting EGFR in lung cancer via ligand-based pharmacophore modeling and*

molecular docking studies. In Silico Pharmacology, 2023. **11**(1): p. 1-27, https://doi.org/10.1007/s40203-023-00157-1.

28. Rauf, A., et al., *Synthesis and urease inhibition studies of barbituric and thiobarbituric acid derived sulphonamides.* Journal of the Chinese Chemical Society, 2011. **58**(4): p. 528-537, https://doi.org/10.1002/jccs.201190017.
29. Taha, M., et al., *Synthesis of new urease enzyme inhibitors as antiulcer drug and computational study.* Journal of Biomolecular Structure and Dynamics, 2022. **40**(18): p. 8232-8247, https://doi.org/10.1080/07391102.2021.1910072.
30. Weatherburn, M., *Phenol-hypochlorite reaction for determination of ammonia.* Analytical chemistry, 1967. **39**(8): p. 971-974, https://doi.org/10.1021/ac60252a045.
31. Ullah, H., F. Khan, and F. Rahim, *Synthesis, in vitro urease inhibitory potential and molecular docking study of thiazolidine-4-one derivatives.* Chemical Data Collections, 2024. **49**: p. 101103, https://doi.org/10.1016/j.cdc.2023.101103.
32. Ahmed, F. and A. Sharif, *A facile single pot synthesis of highly functionalized tricyclic heterocycle compounds via sequential knoevenagel-michael addition and their?-glucosidase inhibition, antioxidants and antibacterial studies.* Journal of the Chemical Society of Pakistan, 2018. **40**(4): p. 761-772, https://inis.iaea.org/search/search.aspx?orig_q=RN:49089064.
33. Shahzadi, T., et al., *Synthesis of eco-friendly cobalt nanoparticles using Celosia argentea plant extract and their efficacy studies as antioxidant, antibacterial, hemolytic and catalytical agent.* Arabian Journal for Science and Engineering, 2019. **44**: p. 6435-6444, https://doi.org/10.1007/s13369-019-03937-0.
34. Rubab, K., et al., *Synthesis, pharmacological screening and computational analysis of some 2-(1H-Indol-3-yl)-N'-[(un) substituted phenylmethylidene] acetohydrazides and 2-(1H-Indol-3-yl)-N'-[(un) substituted benzoyl/2-thienylcarbonyl] acetohydrazides.* Pakistan Journal of Pharmaceutical Sciences, 2017. **30**(4): p. 1263-1275, link.gale.com/apps/doc/A502119138/AONE?u=anon~5327aca0&sid=googleScholar&xid=20d49ef0.
35. Hafeez, J., et al., *Synthesis of N, N-Bis ([1, 1'-Biphenyl]-4-ylmethyl)-4-morpholinoaniline derivatives via SMC reaction: Assessing their anti-seizure potential through electroencephalogram evaluation and molecular docking studies.* Arabian Journal of Chemistry, 2024. **17**(9): p. 1-18, https://doi.org/10.1016/j.arabjc.2024.105889.
36. Azimi, F., et al., *Design and synthesis of novel pyrazole-benzofuran hybrids: in vitro α-glucosidase inhibitory activity, kinetic and molecular modeling study.* Res. Square, 2021: p. 1-22, https://doi.org/10.21203/rs.3.rs-288227/v1.
37. Chaudhry, F., et al., *In search of new α-glucosidase inhibitors: Imidazolylpyrazole derivatives.* Bioorganic chemistry, 2017. **71**: p. 102-109, https://doi.org/10.1016/j.bioorg.2017.01.017.
38. Ibrar, A., I. Khan, and N. Abbas, *Structurally diversified heterocycles and related privileged scaffolds as potential urease inhibitors: a brief overview.* Archiv der Pharmazie, 2013. **346**(6): p. 423-446, https://doi.org/10.1002/ardp.201300041.
39. Liu, H., et al., *Novel coumarin-pyrazole carboxamide derivatives as potential topoisomerase II inhibitors: Design, synthesis and antibacterial activity.* European journal of medicinal chemistry, 2018. **157**: p. 81-87, https://doi.org/10.1016/j.ejmech.2018.07.059
40. Reactivity of benzofuran derivatives, Synthetic Communications 2014, 44(20), 2899-2920.https://doi.org/10.1080/00397911.2014.90742
41. Synthesis of benzofuran derivatives via different methods. Synthetic Communications 2014, 44(16), 2285-2312. https://doi.org/10.1080/00397911.2014.89452
42. Synthesis of new quinoxaline, pyrimidine, and pyrazole furochromone derivatives as cytotoxic agents. Monatshefte für Chemie - Chemical Monthly, 2017,148,1853–1863. DOI: 10.1007/s00706-017-1960-6
43. Synthesis, reactions and biological activities of furochromones: A review. Eur. J. Med. Chem. 2015,633-665. https://doi.org/10.1016/j.ejmech.2014.12.001.
44. Synthesis of New Furothiazolo Pyrimido Quinazolinones from Visnagenone or Khellinone and Antimicrobial Activity. Molecules 2018, 23(11), 2793; https://doi.org/10.3390/molecules23112793
45. Synthesis and Antimicrobial Activity of Novel 1, 2, 4-Triazolopyrimidofuro-quinazolinones from Natural Furochromones (Visnagenone and Khellinone).Medicinal Chemistry 2021,17(7),707-723. https://doi.org/10.2174/1573406416666200406130047